C. R. Chimie 15 (2012) 1012–1021

Contents lists available at SciVerse ScienceDirect

Comptes Rendus Chimie

www.sciencedirect.com

Full paper/Mémoire

Synthesis of gold nanoparticles by microemulsion assisted photoreduction method

Maria Mihaly [a,b], Madalina Camelia Fleancu [a,b], Nicoleta Liliana Olteanu [a], Dionezie Bojin [b], Aurelia Meghea [a,b], Marius Enachescu [b,*]

[a] Faculty of Applied Chemistry and Materials Science, University Politehnica Bucharest, 1 Polizu, 011061 Bucharest, Romania
[b] Center for Surface Science and Nanotechnology, University Politehnica Bucharest, 3Splaiul Independentei, 060042 Bucharest, Romania

ARTICLE INFO

Article history:
Received 21 June 2012
Accepted after revision 27 September 2012
Available online 7 November 2012

Keywords:
Gold nanoparticles
Photoreduction
Microemulsion

ABSTRACT

A new, clean, cost-effective and rapid method for the synthesis of stable spherical gold nanoparticles (AuNPs) is developed. This novel technique combines microemulsion as one of soft-nanotechnology techniques of wet chemistry, with photo-physics of UV-radiation in a unique versatile method to design and obtain controlled nanostructures for multifunctional materials. Based on a phase diagram in ternary water/Brij 30/*n*-heptane system pristine, and thiol functionalized, gold nanoparticles were obtained by a microemulsion assisted photoreduction technique, allowing increased flexibility during the synthesis and selection of materials. The spherical nanoparticles obtained by this route show a homogeneous size distribution, with an average diameter of 11 nm, for pristine gold nanoparticles and of 12 nm, for functionalized species. The evolution of the system at the nanoscale has been studied using, in tandem, UV-VIS and DLS measurements. The structure, size and shape of the final nanoparticles obtained have been evaluated by adequate instrumental techniques: FTIR, XRD and TEM image analysis. Kinetic studies have also been performed in order to follow the evolution of nanospecies during irradiation procedure.

1. Introduction

Metal nanoparticles have become the subject of intensive research because of their scientific and technological importance [1]. As a result of their unique optical, electronic, catalytic and magnetic properties, compared with the corresponding bulk materials, the number of potential applications of these colloidal particles is growing rapidly [2]. Nanoparticles are employed in many fields such as biotechnology, industry, catalysts, optics, life sciences, pharmacy, medicine, mechanics, magnetism and energy science [3].

Due to their unusual properties, synthesis of nanoparticles with specific compositions, sizes, shapes and controlled dispersion is very important.

Some of the most studied nanomaterials with promising applications in many fields are gold nanoparticles [4]. Classical procedure for the synthesis of Au nanoparticles is based on the chemical reduction of tetracloroauric acid with sodium citrate [5]. Nanoparticles with different sizes and morphologies can be synthesized by controlling the reactants, the selection of reducing agent or the addition of the surfactants. There are various methods for gold nanoparticle synthesis, which include electrochemical techniques, synthesis in microemulsion, laser ablation, sonochemistry and sonoelectrochemistry [6–9]. Nevertheless, all these syntheses are time consuming and costly.

One of the most efficient preparation methods, which allows one to control the particle properties such as size, geometry, morphology, homogeneity and surface area, is the water-in-oil (W/O) microemulsion technique [10–12]. Such a system is a well-suitable confined reacting medium for the synthesis of structured functional inorganic nanoparticles of controlled size and shape [13–15]. This

* Corresponding author.
E-mail address: marius.enachescu@upb.ro (M. Enachescu).

1631-0748/$ – see front matter
http://dx.doi.org/10.1016/j.crci.2012.09.013

is a recently developed procedure, which allows preparation of ultrafine mono size and shape nanoparticles with particle diameter range of 5-50 nm [16].

Moreover, a well-known method studied by many researchers as being a clean, cost-effective and convenient technique is the photochemical preparation of gold nanoparticles [17–20].

Combining these two methods, microemulsion and photoreduction, a new technique results, the microemulsion assisted photoreduction (MAPR) method. This procedure benefits from the advantages of microemulsion templates, while, in the same time, uses light as an efficient tool for metallic cations reduction. The main advantages of this method are:

- metal precursor reduction occurs under UV-radiation, reduced chemical consumption and no side effects;
- it gives the possibility to obtain nanoparticles in both water-in-oil (W/O) and oil-in-water (O/W) microemulsion systems which increases the experimental flexibility of this method to confine at nanoscale both hydro- and liposoluble components;
- it is accessible to a wide pallet of metal nanoparticles, ranging from those with positive reduction potential to those with negative potential, or from "bulk" nanoparticles to hollow spheres;
- it can be modified, to a high extent, by adjusting the type or amount of polar/nonpolar phase and surfactants, thus allowing fine adjustment of the micelles and nanoparticle diameter.

This work is focused on the following aspects:

- the preparation of different microemulsion systems and their characterization by using spectral methods and conductivity measurements;
- the control of nature, size and shape of colloidal aggregates (water or oil droplets) templated by microemulsion systems based on size effect revealed on VIS spectra and DLS measurements;
- highlighting a new, clean, cost-effective and rapid method for the synthesis of stable spherical gold nanoparticles (AuNPs), by the microemulsion assisted photoreduction technique.

The evolution of the system at the nanoscale has been described using UV-VIS and DLS measurements, while the structure, size and shape of final nanoparticles obtained have been obtained by adequate instrumental techniques: FTIR, XRD and TEM image analysis.

2. Experimental

2.1. Materials

Hydrogen tetrachloroaurate (HAuCl4), *n*-heptane, polyoxyethylene 4-lauryl ether (Brij 30), triethylene glycol (TEG), sodium 3-mercapto-propanesulfonate (MS) and cysteamine hydrochloride (CS) were purchased from Sigma–Aldrich and bromthymol blue (BTB) was from Chemopal. All chemicals were of analytical grade and used without further purification. Ultra-pure water (Millipore Corporation) was used.

2.2. Synthesis procedure

Gold nanoparticles were synthesized in a water-in-oil microemulsion selected based on a phase diagram built in the water/Brij 30/*n*-heptane system.

In order to find out the region where the microemulsion is formed, a ternary phase diagram (Fig. 1) was constructed using the surfactant titration method at room temperature, following a procedure previously described (Scheme 1) [15].

UV irradiation was carried out with a photoreactor containing a medium-pressure UV lamp at 254 nm. After 1 h irradiation, the microemulsion turns from colorless to dark pink, indicating the formation of AuNPs with specific sizes. The color is defined by the nanoparticle size and shape. Nanoparticles sizes also vary with the precursor concentration.

AuNPs synthesis involves several steps, as shown in Scheme 2.

By using the same method, MAPR technique, thiol functionalized AuNPs have been prepared. Their synthesis involves the preparation of the initial solutions, CS/$HAuCl_4$ and MS/$HAuCl_4$ 0.02 M respectively, both prepared at 25 °C and stirred for 30 minutes. These solutions were subsequently added to the microemulsion with *n*-heptane (82.5% (w/w)) and Brij30 (15% (w/w)).

The resulted NPs were five times alternatively washed with acetone and ethanol in order to remove the oil, surfactant and excess of thiol compounds.

2.3. Instrumental techniques

The evolution of the system at nanoscale has been investigated using, in tandem, UV-VIS, conductivity and DLS measurements, while the structure, size and shape of the final nanoparticles have been obtained by proper instrumental techniques: FTIR, XRD and TEM image analysis.

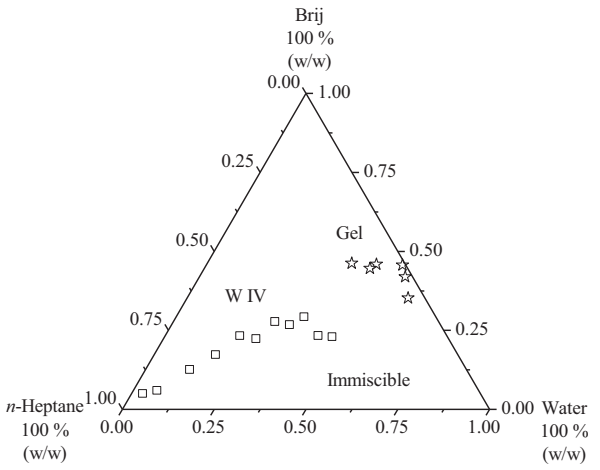

Fig. 1. Ternary phase diagram of the water/Brij/*n*-heptane system at room temperature.
Reproduced with permission from Moldoveanu et al. [11].

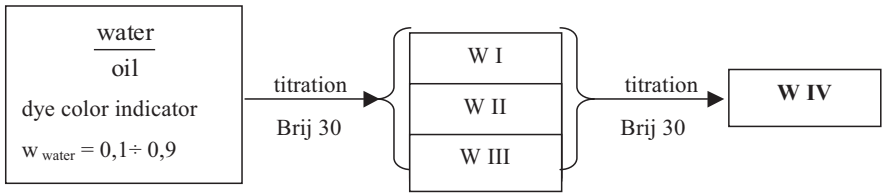

Scheme 1. Construction of phase diagram.

UV-Vis measurements were performed using a Jasco V570 spectrophotometer. For the conductivity measurements, a Consort C831 multi-parameter analyzer was used. Size and zeta potential measurements were made using Malvern Nanosizer equipment. FT-IR measurements were carried out on free and functionalized gold nanoparticles using NICOLET 6700 equipment. The X-ray diffraction pattern of functionalized AuNPs was obtained using a Shimadzu XRD 6000 diffractometer. Morpho-structural characterization of free and functionalized AuNPs was performed using transmission electron microscopy (TEM) Philips EM 410 and for measurement acquisition and performance, dedicated video camera and analysis software were used.

3. Results and discussion

The formation and use of microemulsion of any type, and consequently the nanostructure corresponding to specific applications, requires the delimitation of the interest regions for water/surfactant/oil system by drawing the appropriate phase diagrams.

3.1. Compositional, dynamic and structural effects in ternary water/Brij 30/n-heptane system

A major motivation for this research is the challenge to understand how ordered or complex structures, are formed spontaneously by self-assembly, and how such processes can be controlled in order to prepare structures with predefined size and shape and, as a consequence, predetermined properties.

3.1.1. Construction of phase diagram

Prior synthesis, the phase diagram has been obtained in water/Brij 30/*n*-heptane ternary system at room temperature, in order to select the optimum system and composition domain for AuNPs synthesis in water-in-oil microemulsion template (Fig. 1).

The left side of the diagram mainly corresponds to an organic solution of surfactant, the water being present only in small amounts, corresponding to a system of reverse micelles (RM). The right side of the diagram corresponds to an aqueous surfactant gel containing small amounts of heptane. The dispersion of water droplets into the oil phase or of oil droplets in water increases proportionally with the surfactant concentration for a given water/oil volumetric ratio, $R = V_W/V_O$.

3.1.2. Identification of phase inversion point of water/Brij 30/n-heptane system

The phase diagrams permit a rigorous selection of the optimal composition to carry out the nanoparticles synthesis in microemulsion. More precisely, if the process occurs in a polar, aqueous medium, the areas of interest are Winsor II (W/O, W) and Winsor IV (W/O), while in a nonpolar, organic medium, the zones are Winsor I (O/W, O) and Winsor IV (O/W). These changes can be monitored by

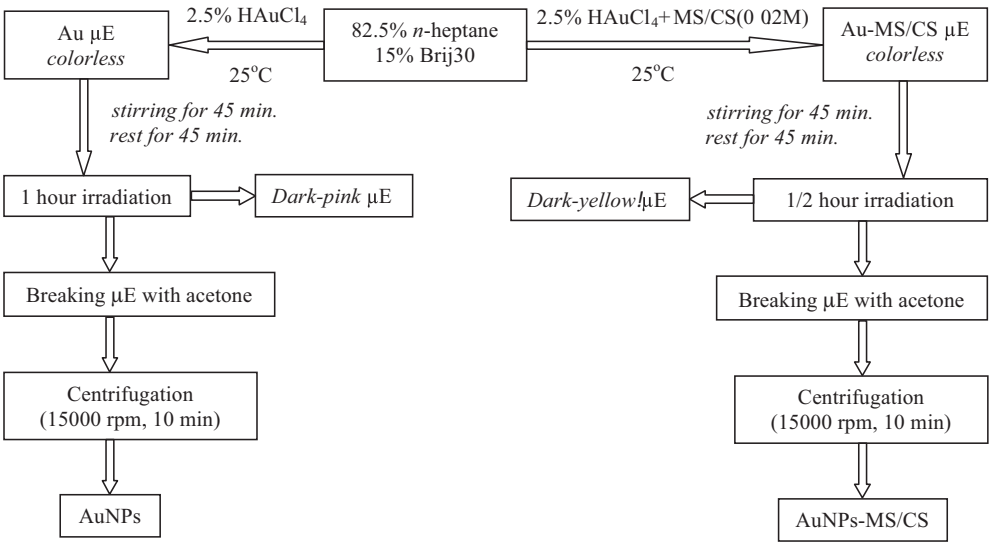

Scheme 2. Schematic preparation diagram of pristine and thiol functionalized AuNPs synthesis.

Table 1
Compositions of the tested W IV microemulsions with various water/oil volumetric ratios, R.

R	0.03	0.05	0.11	0.18	0.25	0.33	0.43	0.54	0.67	0.82	1.00
Brij % (w/w)	4.7	5.7	12.3	17.0	23.0	22.1	27.5	26.5	29.0	23.1	22.7
Water % (w/w)	3.4	6.8	12.4	17.1	20.7	25.6	28.0	32.5	35.2	42.0	46.0
Heptane % (w/w)	91.9	87.5	75.3	65.9	56.3	52.3	44.5	41.0	35.8	34.9	31.3

Reproduced with permission from Moldoveanu et al. [11].

using an indicator, in our case bromthymol blue (BTB) dye, which allow one to build the phase diagram by spectral measurements in the visible domain.

In order to characterize the systems with water nanodroplets dispersed into the oil phase (W/O), several WIV fluid microemulsions of different compositions were prepared (Table 1) and characterized by VIS spectroscopy (Fig. 2(a)) and electrical conductivity measurements (Fig. 2(b)). Spectral investigation is based on solvatochromic effect that cannot be found in rigid samples such as aqueous surfactant gel containing small amounts of heptane ($R > 1$), so studies have been limited to systems corresponding to $R < 1$.

The shift of the absorption maxima of electronic band in visible domain for microemulsions with various compositions is represented in Fig. 2(a). The band wavelengths increase starting from the absorption maxima of the BTB dye indicator in Brij ($\lambda_{max} = 408$ nm) to that in TEG ($\lambda_{max} = 416$ nm). This behavior suggests the hydration of the oxyethylene groups and consequently, the formation of a W/O microemulsion. By increasing the water content, $R = V_W/V_O \sim 0.3$, the repulsive forces between oxyethylene groups of the surfactant molecules become predominant and the wavelength shifts to the absorption maxima of BTB dye in Brij ($\lambda_{max} = 408$ nm) are observed. This hypsochromic effect is associated with the phase inversion point, when the O/W microemulsion occurs, and a mixture of bicontinuous W/O and O/W microemulsions is formed.

Therefore, the BTB dye molecules are, in both cases, solubilized into the colloidal aggregates core, as they are almost insoluble in any of these two solvents, water and heptane, when the surfactant is absent.

According to the spectral measurements, the phase inversion point, from water-in-oil to a mixed microemulsion, can be also assigned at $R = V_W/V_O \sim 0.3$ and corresponds to the slope change in the conductivity values of the volumetric water/oil ratio (Fig. 2(b)). The second slope change would be attributed to the inversion from a mixed to oil-in-water microemulsion.

3.1.3. Size effect on fluid nanostructures

The nanostructure characteristics have a length scale in the low nanometers range that influences their physical or chemical properties. Their novel or unusual physical properties are mainly due to finite-size effect: electronic bands are gradually converted to molecular orbital as the size decreases.

The difference in the peak position of electronic spectra is related to the size effect of the nanostructured units in the bulk phase. When a three-dimensional square-well potential with the length of L in x, y and z directions is in the quantum size, the energy of an electron, ΔE, confined within a potential well can be given by the following equation [20]:

$$\Delta E = \frac{3 \cdot \hbar^2 \cdot \pi^2}{2 \cdot m \cdot L^2}, \hbar = \frac{h}{2\pi} \quad (1)$$

where m is the static mass of an electron (9.10938×10^{-31} Kg), and h is the Planck constant (6.62608×10^{-34} J·s).

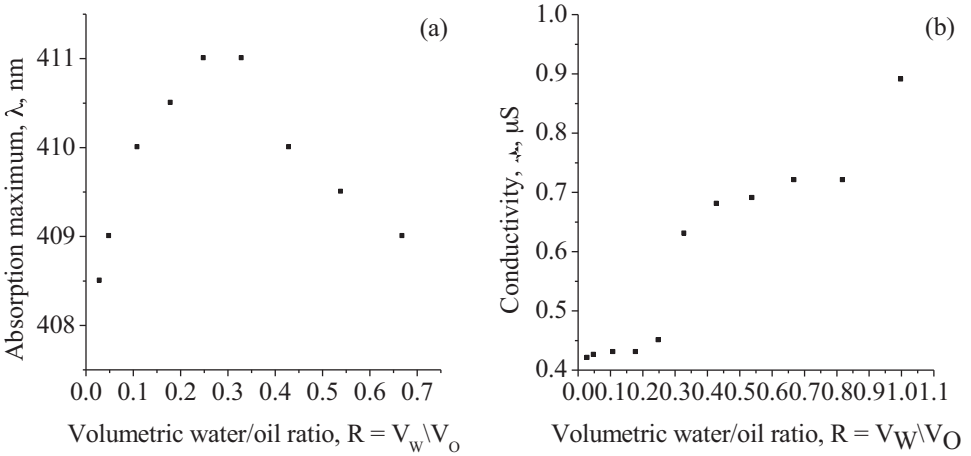

Fig. 2. Absorption maxima wavelength (a) and electrical conductivity (b) dependence on the water/oil volumetric ratio, *R*.
Reproduced with permission from Moldoveanu et al. [11].

Table 2
Size estimation based on VIS and DLS spectra of W/O microemulsions.

$r = W_W/W_{Brij}$	0.06	0.13	0.15	0.19	0.26	0.37	0.56	0.72	1.19
L_{VIS} nm (VIS spectra)	4.0	5.0	5.3	6	6.5	7.8	10.2	12.5	17.7
L_{DLS} nm (DLS spectra)	4.3	5.1	5.5	5.9	6.7	7.5	9.8	11.9	17.5
Polydispersity	0.113	0.109	0.214	0.203	0.195	0.201	0.254	0.179	0.158

Reproduced with permission from Moldoveanu et al. [11].

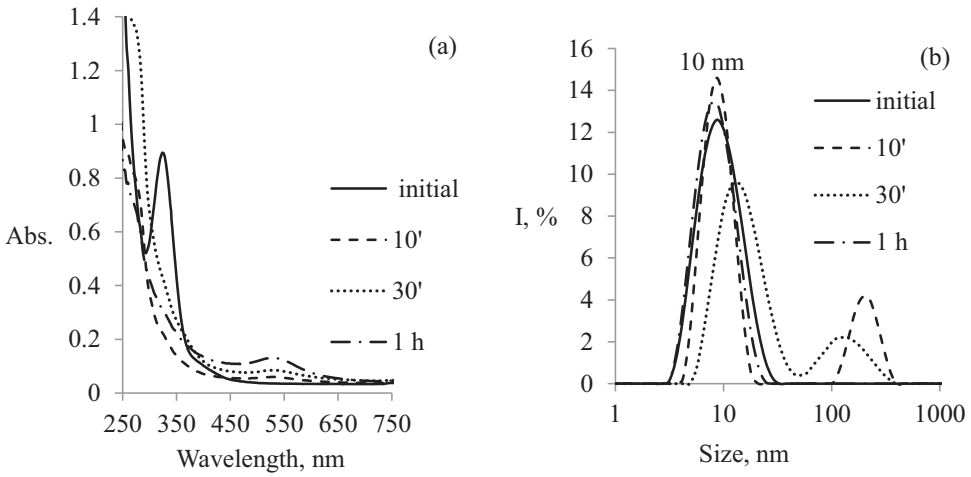

Fig. 3. Kinetics of pristine AuNPs formation: (a) evolution in time of electronic spectra; (b) evolution in time of particle size.

Since the phase inversion point is around $R = 0.3$, and W/O microemulsions are involved in inorganic nanoparticles preparation, several compositions, corresponding to different water/surfactant mass ratio, $r = W_W/W_{Brij}$ have been prepared (Table 2). These microemulsions have been further used to determine the size of the water droplets dispersed into the heptane liquid phase in order to decide if their size could be controlled by changing the concentration of the surfactant.

The size of the aggregates in micelles, L, may be obtained from ΔE (Eq. (1)) which is the difference between the spectral position of BTB peak in TEG (hydrated oxyethylene groups) (416 nm) and that in microemulsions (Table 2). The results for droplet size, ranging between 4-17.5 nm, obtained from VIS spectra are in a good agreement with DLS measurements and follow the size dependence of water/surfactant mass ratio, r.

3.2. DLS and UV-Vis measurements for AuNPs preparation

The results of this section provide information about the evolution of nanoparticle size at different irradiation time, thus allowing a qualitative kinetic study for the photoreduction reaction of gold ions in microemulsion. From DLS measurements (Fig. 3(b)) one can be seen that colloidal aggregates are maintaining their initial shape and size (about 10 nm), even after irradiation, suggesting that AuNPs take their geometrical characteristics. AuNPs formation is marked by microemulsions staining, compared to baseline, when it is colorless. The presence of larger aggregates (60-100 nm) during irradiation, up to 1 h, is attributed either to the formation of aggregates by nanodroplets breaking with increasing irradiation time or to the existence of both free micelles and gold nanoparticles in the sample.

A simultaneous analysis of the evolution in time of the electronic spectra (Fig. 3(a)) and particles size (Fig. 3(b)) during pristine AuNPs formation reveals similar aspects. Initial gold microemulsion (Au μE) spectra, before irradiation, show a maximum absorption at 325 nm, which is characteristic for $[AuCl_4]^-$ micelles of 10 nm size. This band can be attributed to a strong charge transfer transition (CT) specific to $[AuCl_4]^-$ species. After 10 minutes of irradiation, this peak disappears and a new band evolves at 532 nm, characteristic for gold nanoparticles of 10 nm size followed by a systematic increase for the peak from 532 nm during the irradiation. This effect is accompanied by formation of a second peak in the DLS spectrum at 200 nm size (Fig. 3(b)) up to 1 h of irradiation, while at 1 h, this peak disappeared following the establishment of thermodynamic equilibrium and the final AuNPs size seems to be similar to that of micelles templates, about 10 nm.

Kinetic processing of absorption spectra at specific wavelengths, i.e., at 325 nm for Au μE and 532 nm for gold AuNPs μE, indicates a complex mechanism, involving

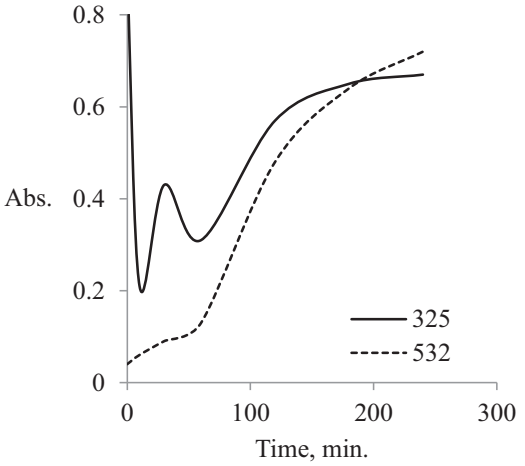

Fig. 4. Kinetic analysis for pristine AuNPs.

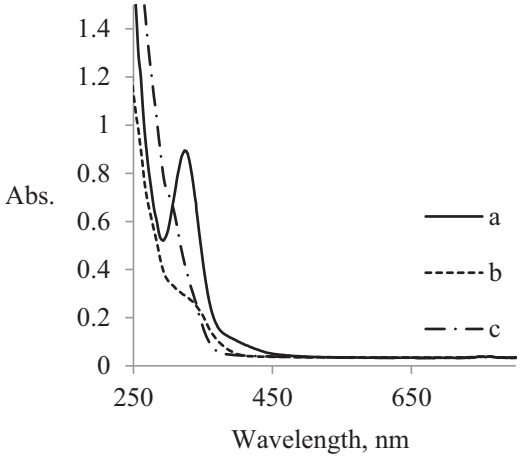

Fig. 5. UV spectra for Au μE before irradiation: a: Au μE; b: Au-MS μE; c: Au-CS μE.

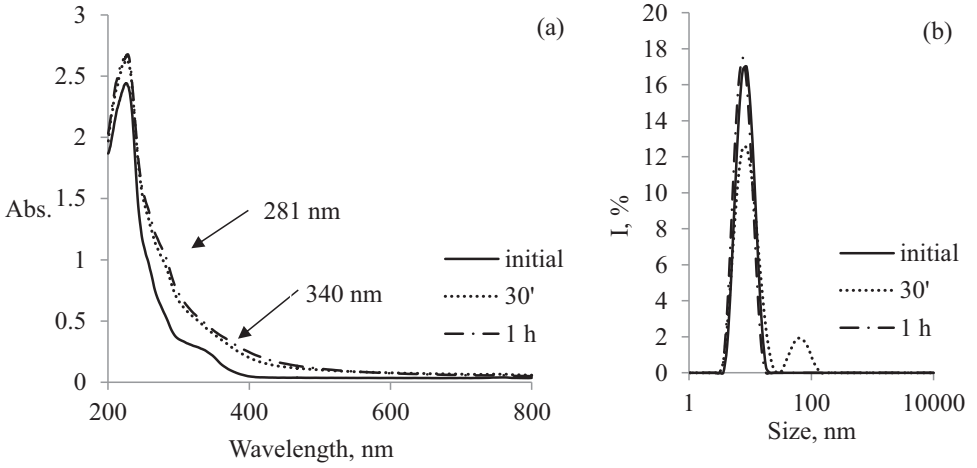

Fig. 6. Evaluation in time of AuNPs-MS: (a) electronic spectra; (b) DLS spectra.

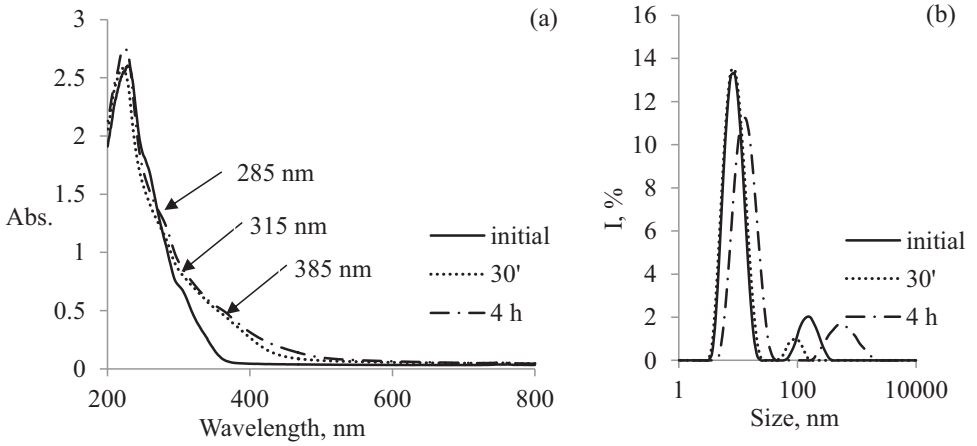

Fig. 7. Evolution in time of AuNPs-CS: (a) electronic spectra; (b) DLS spectra.

initial micelles transformation into a series of AuNPs with various sizes during the first hour of irradiation (Fig. 4). After further irradiation, until 4 h, equilibrium between initial micelles and AuNPs of similar sizes is observed. This behavior is shown by the sinuous region of spectral absorption corresponding to λ = 325 nm in the first 50 minutes, concomitant with the presence of an induction period for AuNPs formation, which is specific to a final product obtained in a system with successive processes.

The effect of thiol-functionalization with 3-mercapto-propanesulfonate (MS) on electronic spectra of Au μE before irradiation is shown in Fig. 5.

After the functionalization with mercapto groups, the intensive CT band specific to $[AuCl_4]^-$ at 325 nm disappeared and it remains only as a "shoulder" at 339 nm for MS derivative and at 308 nm for CS derivative. These hipso- and hipocromic effects are specific for replacing –SH groups with Au-S coordination bonds in mercapto-functionalized micelles.

The formation of AuNPs-MS nanoparticles can be revealed by the "shoulder" from 281 nm and its spectral evolution is similar to that for pristine AuNPs (Fig. 6(a)). During the first 30 minutes, nanoparticles with 50–60 nm sizes are formed, which are stabilized after 1 h of irradiation at sizes similar with those of initial micelles around 13 nm (Fig. 6(b)).

For AuNPs-CS (Fig. 7), inhomogeneous polydisperse systems are obtained after 4 hours of irradiation. The

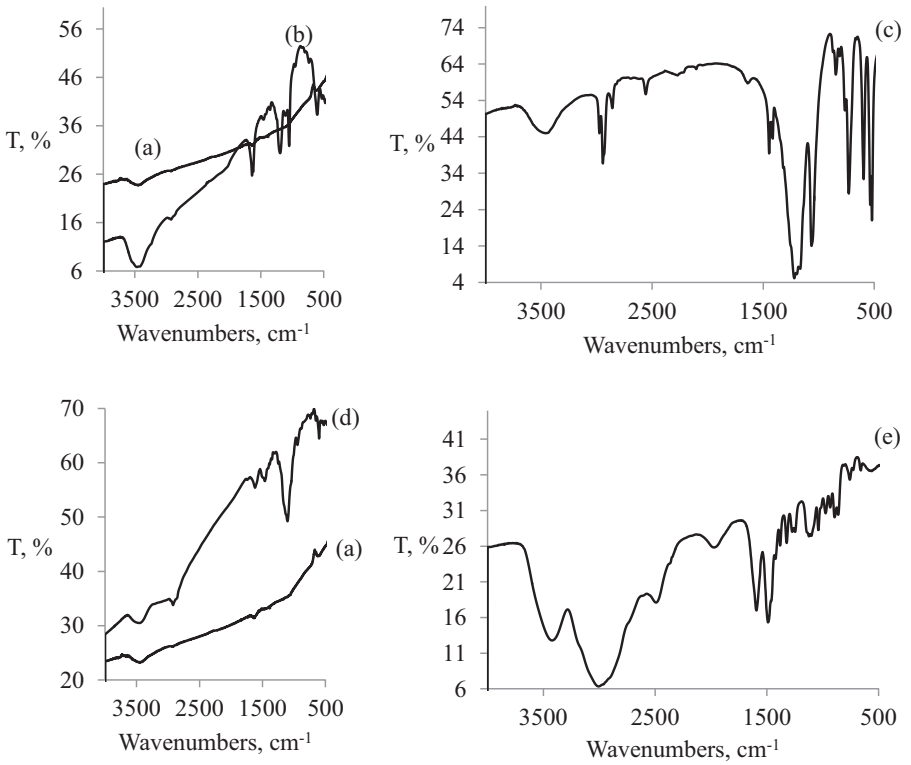

Fig. 8. FT-IR spectra of (a) AuNPs; (b) AuNPs-MS; (c) MS powder; (d) AuNPs-CS; (e) CS powder.

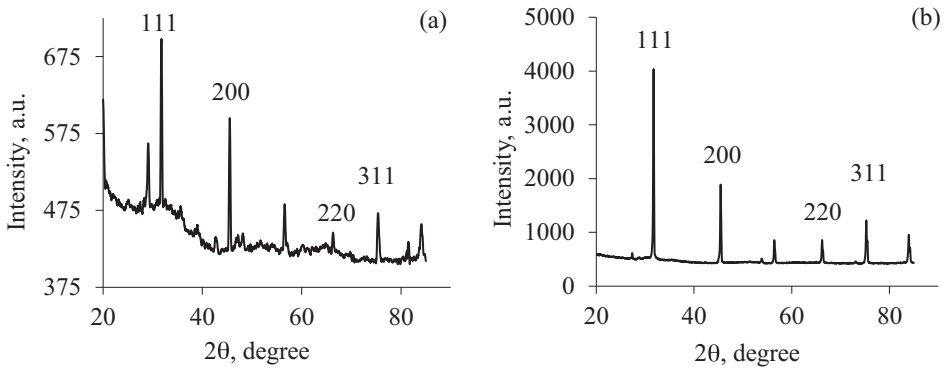

Fig. 9. XRD pattern of (a) AuNPs-MS and (b) AuNPs-CS.

stability of nanoparticles is lower than that observed for AuNPs functionalized with MS.

Table 3 shows Zeta potential values for water dispersed pristine and functionalized AuNPs, which is a stability indicator for colloidal solutions. If all AuNPs species present in suspension have high, either negative or positive

Table 3
The Zeta potential values for water dispersed simple and functionalized AuNPs.

Sample	AuNPs	AuNPs-CS	AuNPs-MS
Zeta potential, mV	22.64	27.13	37.73

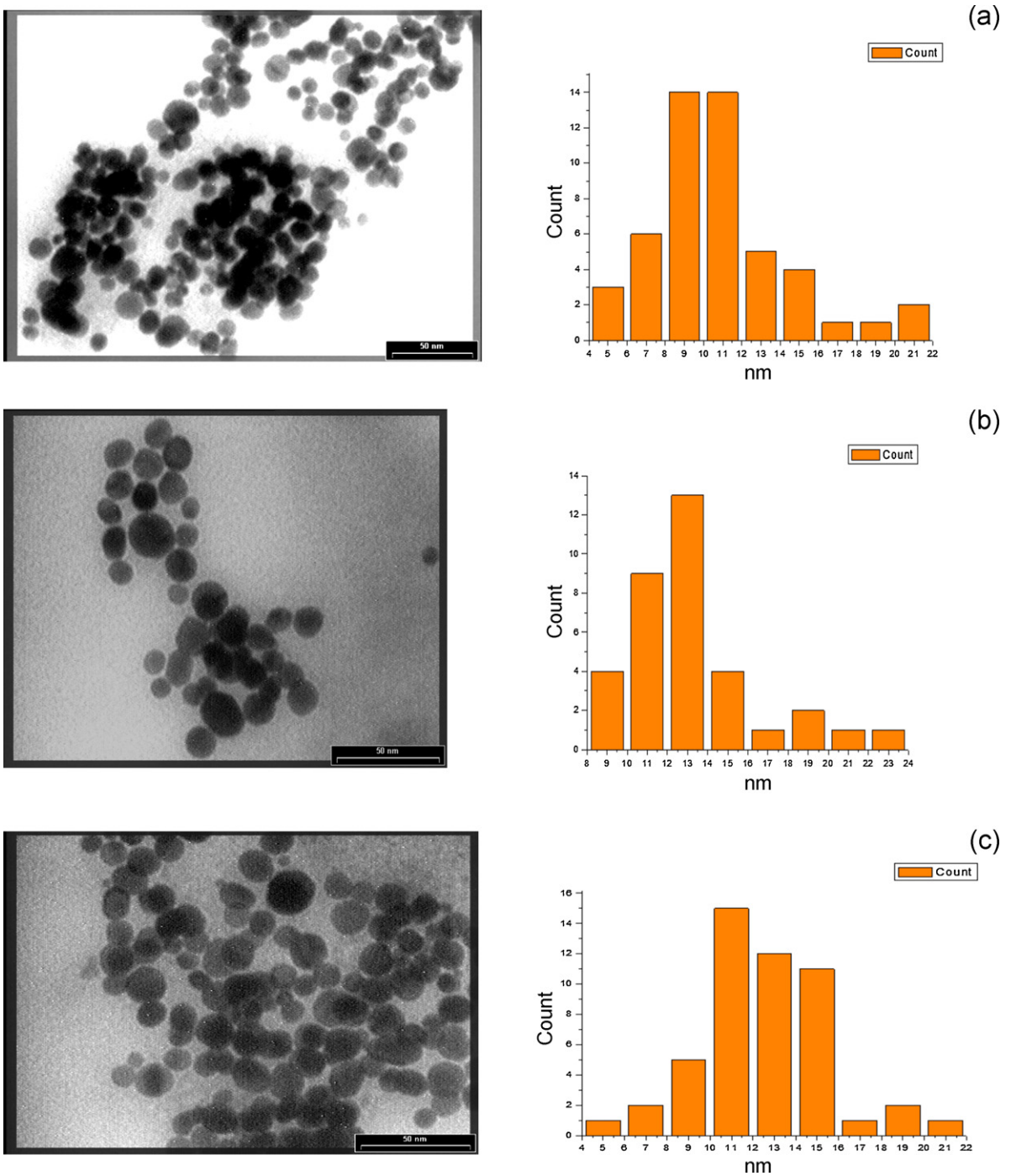

Fig. 10. TEM images and size statistical distribution of (a) pristine AuNPs; (b) AuNPs-MS; (c) AuNPs-CS.

Zeta potential values (outside the range $-30 \div +30$ mV), they tend to repel each other and to avoid aggregation. Therefore, small Zeta potential values suggest a tendency to aggregation.

The results obtained indicate that pristine AuNPs in water dispersion have moderate stability. After functionalizing them with thiols like CS, the stability is slightly improved, while for MS, they become much more stable.

3.3. Morpho-structural characterization of functionalized AuNPs

3.3.1. FT-IR spectroscopy

FT-IR spectra for functionalized AuNPs are presented in Fig. 8 as compared with pristine gold nanoparticles and corresponding mercapto-derivative.

All three types of gold nanoparticles have similar patterns as can be seen from to the big slope of the baseline and the absence of significant vibrations in the case of pristine AuNPs (Fig. 8(a), (b) and (d)).

However, the stretching $\nu_{S\text{-}H}$ band, clearly present in free CS at 2550 cm^{-1} (Fig. 8(c)), is absent in AuNPs-CS (Fig. 8(d)), thus confirming once again the functionalization through Au-S coordination bond.

Moreover, in case of MS, the most intensive bands of organic ligand, specific to SO_3 group at 1064 (ν_3), 1219 (ν_1) (Fig. 8(c)) are also present as fingerprints in AuNPs-MS, shifted at 1048 and 1192 cm^{-1} (Fig. 8(b)). Even weaker bands specific to methylenic groups, ν_{CH2} at 2848 and 2920 cm^{-1} are still present in AuNPs-MS, while the stretching $\nu_{S\text{-}H}$ band present in MS, actually disappeares in AuNPs-MS. This confirms the formation of Au-S coordinative bond during functionalization.

3.3.2. XRD analysis

XRD patterns for functionalized AuNPs present almost the same characteristics as metallic gold and indicate the presence of some peaks, whose values correspond to Miller indices specific for gold, respectively (111), (200), (220), (311) (Fig. 9(a), (b)). By comparing these values with the crystallographic data basis, it can be seen that AuNPs crystallize into a face-centered cubic (fcc) phase of metallic gold. The *amorphous* hollow surrounding the thiol functionalized gold nanoparticles would be assigned to the ligand shell physically adsorbed on the gold nanoparticles surface.

3.3.3. TEM studies

The shape and size distribution of the AuNPs were determined and confirmed by transmission electron microscopy (TEM) (Fig. 10).

Fig. 10 show typical TEM images and the corresponding size distribution histogram of the synthesized gold nanoparticles.

One can be seen that all AuNPs are spherical in shape, well separated from each other, with only a small amount of conglomerates.

Size distribution histograms of all AuNPs correspond to a normal distribution and show that the average size is 11 nm for pristine AuNPs, 12 nm for AuNPs-CS and 13 nm for AuNPs-MS, in good agreement with DLS measurements.

4. Conclusions

Microemulsion assisted photoreduction (MAPR) technique, a new, clean, low cost and easy to handle method developed and implemented in our lab, is proven synthesizing pristine and thiol functionalized gold nanoparticles.

By using the microemulsion template, the agglomeration of the resulting nanoparticles is avoided. The role of thiol ligands is to promote the nanoparticles dispersion into aqueous media and thus to prevent their agglomeration in the microemulsion liquid phase.

All AuNPs prepared in this way are crystallized into a face-centered cubic (fcc) phase, monomodal, spherical, about 10 nm diameter, well dispersed into aqueous media, which make them appropriate for biological applications.

Compared to other synthesis methods, MAPR technique seems to be more accessible since it does not require a high quantity of reagent, the use of hazardous and/or toxic solvents and allows a greater flexibility in tuning the synthesis parameters.

On the whole, this novel technique combines microemulsion, as one of soft-nanotechnology techniques of wet chemistry, with photo-physics of UV-radiation into a unique versatile method to design and obtain controlled nanostructures for multifunctional materials.

Acknowledgements

The work has been funded by the Sectoral Operational Programme Human Resources Development 2007–2013 of the Romanian Ministry of Labour, Family and Social Protection through the Financial Agreement POSDRU/88/1.5/S/61178.

This work was supported by UEFISCDI, ERANET contract no. 4_001/7.04.2011, project acronym NANODIATER under the frame of EuroNanoMed.

References

[1] B. Wu, Y. Kuang, X. Zhang, J. Chen, Nano Today 6 (2011) 75.
[2] J. Zhou, J. Ralston, R. Sedev, D. Beattie, J. Colloid Interf. Sci. 331 (2009) 251.
[3] K.B. Narayanan, N. Sakthive, Adv. Colloid Interfac. 156 (2010) 1.
[4] Z. Liang, J. Zhang, L. Wang, S. Song, C. Fan, G. Li, Int. J. Mol. Sci. 8 (2007) 526.
[5] J. Turkevich, P.C. Stevenson, J. Hillier, Discuss. Faraday Soc. 11 (1951) 55.
[6] V.C. Ferreira, J. Solla-Gullón, A. Aldaz, F. Silva, L. Abrantes, Electrochim. Acta 56 (2011) 9568.
[7] A. Toyota, T. Sagara, Electrochim. Acta 53 (2008) 2553.
[8] C.M. Sanchez-Sanchez, F.J. Vidal-Iglesias, J. Solla-Gullon, V. Montiel, A. Aldaz, J.M. Feliu, E. Herrero, Electrochim. Acta 55 (2010) 8252.
[9] J. Kimling, M. Maier, B. Okenve, V. Kotaidis, H. Ballot, A. Plech, J. Phys. Chem. B 110 (2006) 15700.
[10] I. Lacatusu, M. Mihaly, I.A. Enesca, A.A. Meghea, Mol. Cryst. Liq. Cryst. 483 (2008) 228.
[11] M. Moldoveanu, I. Rău, M. Fleancu, M. Mihaly, U.P.B. Sci. Bull. Series B 73 (2011) 41.
[12] T. Aubert, F. Grasset, S. Mornet, E. Duguet, O. Cador, S. Cordier, Y. Molard, V. Demange, M. Mortier, H. Haneda, J. Colloid Interface Sci. 341 (2010) 201.

[13] M. Mihaly, A. Comanescu, A. Rogozea, E. Vasile, A. Meghea, Mat. Res. Bull. 46 (2011) 1746.
[14] M. Mihaly, A. Rogozea, A. Comanescu, E. Vasile, A. Meghea, J. Optoelectron. Adv. Mat. 10 (2010) 2097.
[15] I. Capek, Adv. Colloid Interfac. Sci. 110 (2004) 49.
[16] M. Sakamoto, M. Fujistuka, T. Majima, J. Photoch. Photobio. C140 (2007) 153.
[17] W. Hao, W. Yang, W. Huang, G. Zhang, Q. Wu, Mater. Lett. 62 (2008) 3106.
[18] X. Qin, W. Lu, G. Chang, Y. Luo, A.M. Asiri, A.O. Al-Youbi, X. Sun, Gold Bull. 37 (2004) 3.
[19] T.K. Sau, A. Pal, N.R. Jana, Z.L. Wang, T. Pal, J. Nanopart. Res. 3 (2001) 257.
[20] P. Atkins, J. de Paula, Physical Chemistry, Seventh ed., University Press, Oxford, 2006.